PSFC/JA-05-34

Internal Transport Barriers in Alcator C-Mod

C. L. Fiore; D. R. Ernst; J. E. Rice;
K. Zhurovich; N. Basse;
P. T. Bonoli; M. J. Greenwald;
E. S. Marmar; S. J. Wukitch

August, 2005

Plasma Science and Fusion Center
Massachusetts Institute of Technology
Cambridge, MA 02139

Internal Transport Barriers in Alcator C-Mod

C. L. Fiore, D. R. Ernst, J. E. Rice, K. Zhurovich, N. Basse, P. T. Bonoli, M. J. Greenwald, E. S. Marmar, S. J. Wukitch, MIT-PSFC

Abstract

Internal transport barriers, marked by steep density and pressure profiles and reduction of core transport are obtained in Alcator C-Mod. Transient single barriers are observed at the back transition from H- to L- mode, and also when pellet injection is accompanied by ICRF power. Double barriers are induced with injection of off-axis ICRF power deposition. These also arise spontaneously in Ohmic H-mode plasmas when the H-mode lasts for several energy confinement times. C-Mod provides a unique platform for studying such discharges: the ions and electrons are tightly coupled by collisions with Ti/Te=1, and the plasma has no internal particle or momentum sources. ITB plasmas with average pressure greater than 1 atmosphere have been obtained. To form an ITB, particle and thermal flux are reduced in the barrier region, allowing the neoclassical pinch to peak the density while maintaining the central temperature. Gyrokinetic simulation suggests that long wavelength drift wave turbulence in the core is marginally stable at the ITB onset, but steepening of the density profile destabilizes trapped electron (TEM) modes inside the barrier. The TEM ultimately drives sufficient outgoing particle flux to balance the inward pinch and halt further density rise, which allows control of particle and impurity peaking.

I. *Introduction*

The presence of internal transport barriers has been noted under a number of different operational regimes in Alcator C-Mod[1,2,3,4,5,6,7]. They are most notable in the plasma density profile which displays strong peaking with a distinctive break in the profile near the plasma half radius, indicating that a strong barrier to particle transport has formed. The pressure profile also displays strong gradients which implies that no loss in thermal energy is occurring as the core density rises, indicates that a thermal barrier exists in the plasma interior as well.

In this paper, we will review the experimental observations of ITBs in Alcator C-Mod that are established by such means as pellet injection, H- to L-mode back transitions, induction with off-axis ICRF power distribution, and in Ohmic H-modes. The common elements of these will be compared, along with discussion of the transport analysis. A review of the gyrokinetic simulations of the C-Mod ITBs will conclude the paper.

II. *Alcator C-Mod ITBs*

II.1 Pellet enhanced performance

Transport barriers in the core plasma region were first reported following the injection of frozen hydrogen pellets into the Alcator C tokamak[8,9]. Strong central density peaking accompanied by a marked improvement in the energy confinement of the

plasma was reported following the injection of both frozen hydrogen and deuterium pellets. It was observed that particle transport and thermal ion transport reduced to near neoclassical levels.

On Alcator C-Mod, Li pellets (typically 1 x 10^{20} electrons) have been injected in combination with on-axis ICRF heating to obtain the transport barrier associated with pellet enhanced performance or PEP mode[10,11]. The best results are obtained when the pellet is injected prior to the ICRF turn-on, so that the pellet can better reach the plasma center. The high density also enhances the focusing of the central ICRF deposition. As shown in Fig 1, the PEP mode is characterized by a strong enhancement in the fusion neutron production, plasma stored energy, and central plasma pressure. The evolution of the density profiles is shown in Fig. 2 comparing the pre- and post-pellet profile. The PEP mode is transient, in this case ending 0.11 s following the injections of pellet[2].

Imaging of the lithium pellet ablation trail has been used to measure the total magnetic field angle as the pellet traverses the plasma[10]. This information was used in conjunction with EFIT[12] equilibrium reconstruction to obtain current density and q profile during PEP mode. The resulting q profile, measured 0.075 s after the pellet injection, 0.01 ms after the peak in the neutron production, was found to be hollow with q_0 =2 and q_{min} slightly above 1 at r/a =0.4. The current density profile is consistent with TRANSP calculations showing ¼ of the current at ρ=0.3 attributable to the bootstrap current for this case.

II.2 Enhanced neutron mode

The profile evolution shown in Fig. 3 is characteristic of the enhanced neutron (EN) mode, a short lived ITB event which occurs shortly after the plasma makes a transition from H- to L-mode. The profile shown here of the electron density, n_e, is derived from the profiles of the visible bremsstrahlung radiation[13] ,$V_b = n_e^2 * Z_{eff}$. Z_{eff} is the average charge state of the plasma and is between 1 and 2 for most Alcator C-Mod plasmas. Comparison of V_b to the density obtained from Thomson scattering in this case indicates that Z_{eff} has a flat radial profile as is typical for most operation.

The EN mode is characterized by a large increase in the neutron rate, where increases of up to 8 times have been observed. The usually flat density profile characteristic of H-mode plasmas, including an edge pedestal, is shown immediately prior to the transition in Fig 3.a. In short order, the density collapses in the outer region of the plasma while the central value is unchanged, temporarily resulting in a strongly peaked radial density distribution. The density in the outer part of the plasma flattens (Fig 3.b) while the central density remains peaked indicating that a transport barrier has formed. During this time, the neutron production rate increases sharply (Fig 3.d) indicating that the central ion temperature is increasing. The enhanced neutron rate persists at an elevated level through several sawtooth cycles, even beyond the point in time where the central density collapses, re-establishing a flat L-mode density profile (Fig. 3.c).

EN mode is seen following the majority of H-to L-mode transitions, in both ICRF and Ohmic plasmas. Data from a typical Alcator C-Mod H- to L-mode transition are shown in Fig. 4. The global neutron rate is shown in the top trace, following the transition. It is indicative of an increase in the central ion temperature because the central density is steady and the line average density is decreasing. Ion temperature profile data on Alcator C-mod, obtained from a scannable array of 5 high spectral resolution x-ray spectrometers (HIREX)[14], are typically measured with 0.1 s time resolution, which is not sufficient to resolve these short lived core barrier effects. However, by purposely triggering H- to L-mode transitions in similar discharges and averaging data for several pulses, the ion temperature profiles shown in Fig. 5 were obtained with 0.02 s resolution. The central ion temperature measured in this manner is higher following the end of the H-mode; however, the profile is not noticeably more peaked than the profile obtained in the H-mode phase. Gaussian fits to the data are included in the figure, and the 1/e width shows no significant change.

Calculation of the scale length ratio η_x (defined as $d \ln T_x / d \ln n_x$ or L_n/L_T; $L_n = \{1/n_x |d\, n_x/dr|\}^{-1}$; $L_T = \{1/T_x |d\, T_x/dr|\}^{-1}$) shows that variation in this parameter results from changes in L_n. There are not sufficient ion temperature profile data to determine η_i for most of the data set, but η_e can be easily obtained from spatially resolved measurements of T_e obtained from electron cyclotron emission as well as from Thomson scattering. Because of the high density operation in Alcator C-Mod, T_e and T_i are equal

within experimental error, and η_e is used as a surrogate for η_i . η_e was calculated at the H to L mode transition for many events which showed the characteristic ITB formation and it was found η_e consistently drops to a value between 1 and 2 at the time that the neutron rate peaks as in Fig 6.

II.3 Off-axis ICRF

Non transitory ITBs, lasting ten or more energy confinement times also arise in Alcator C-Mod. These occur when long-lived enhanced D_α H-modes (EDA) are established in which the net central power is not peaked on axis. This is common in H-mode plasmas which have been formed when ICRF power is injected into the plasma with the resonance location placed off-axis, on either the low or high field side of the plasma. The best results are obtained with the resonance position located at or slightly greater than r/a=0.5. An example of density profiles derived from visible bremsstrahlung radiation is shown in Fig. 7. A calculation of the ICRF power deposition profile is also included in that figure. Note that the ITB foot position falls well inside of the ICRF power peak. Z_{eff} becomes somewhat centrally peaked when a strong ITB is present, as can be seen from calculating the ratio of the square root of the visible bremsstrahlung emission with the density profile obtained from Thomson scattering. This is shown in Fig 8. Central Z_{eff} ultimately reaches a value of 3.0 late in the ITB phase of the discharge, just before the H-mode undergoes a back transition to L-mode.

Alcator C-Mod H-mode plasmas demonstrate strong co-going central plasma rotation. The magnitude of the velocity has been shown to be dependent upon the plasma stored energy and the current [15]. It has been widely reported that this co-going rotation slows and reverses to the counter direction as a typical ITB develops in these plasmas[1,3,5]. An example of the rotation velocity is compared for two similar discharges in Fig. 9. In both cases ICRF power of 3 MW is turned on at t = 0.7 s, and the plasma enters into H-mode almost immediately. In the case represented by the dashed line, the toroidal field was 4.9 T and the RF resonant layer was slightly off-axis on the high field side. The ratio of central electron density to that from one of the outer channels from the same shot shows no peaking throughout the H-mode phase of the plasma. The solid trace in both figures is from a plasma with the same conditions, except that the toroidal field was at 4.5 T, bringing the RF resonance layer to r/a=0.5, in the region where the ITB is typically formed in the Alcator C-Mod core. As can be easily seen, the rotation started to rise when the ICRF power was turned on at 0.7 s, and then it began to decrease monotonically 0.2 s later. Shortly thereafter, the density peaking factor increases indicating that an ITB has formed. In ITBs formed at high field with high ICRF input power, the rotation decreases as the ITB forms but it does not reverse[7].

The formation of the ITB is extremely sensitive to the applied toroidal magnetic field, suggesting that the location of the ICRF resonance position is critical for an ITB to arise. In Fig. 10, the toroidal field is scanned such that the resonance position for the 70 Mhz

ICRF power moves from r/a>0.5 on the high field side to r/a >0.5 on the low field side. As indicated by the peaking factor and the value of the central toroidal rotation, ITBs form when the resonance position reaches the extreme values on either side of the plasma. Other experiments suggest that changes in the applied magnetic field of even less than 1% can influence whether or not an ITB is formed. First, an H-mode is established using off-axis ICRF power at a toroidal magnetic field value which locates the ICRF resonance too close to the center for ITB development. In a subsequent experiment, the toroidal magnetic field is then ramped down, which moves the resonance farther towards the high field side of the plasma, effectively to larger r/a position, until an ITB is produced. The converse is also done, in which an ITB is established in an off-axis ICRF heated plasma with the magnetic field ramping up until the ITB profile is lost. Since the location of the ICRF power deposition is changed with the magnetic field ramp, it seems reasonable to suggest that the most important factor in this test is the relative amount of power located inside/outside of the ITB radius. The total of the Ohmic and ICRF power distribution (calculated with TRANSP using the TORIC code[16] coupled to a Fokker-Planck solver) in these plasmas is shown in Fig. 11. The ITB forms in these experiments when the power inside the ITB radius is roughly less than 40% of the total input and that the ITB terminates when the power inside the ITB radius exceeds 60% of the total.

II.4 Ohmic H-mode

The core density and pressure increase characteristic of ITB development occurs spontaneously in Ohmic H-mode operation when an EDA H-mode is sustained for at

least 2 energy confinement times. This suggests that the ITB formation is not triggered by the RF itself, but is likely to result from a particular parametric profile. An example is shown in Fig. 12. The peaked density shown here arose spontaneously after the plasma went into H-mode. The Ohmic H-mode is typically induced by ramping the toroidal magnetic field down to a low value in order to lower the H-mode threshold. Typically the plasma sawtooth activity slows and stops as the density peaks, suggesting that q_0 exceeds 1 for at least part of this event. In this case the ITB lasted more than 400 ms, at least 10 energy confinement times, ending only as the plasma current began to ramp down in a controlled termination of the discharge. As in the off-axis ICRF heated ITB, the central toroidal rotation is seen to decline as the ITB develops.

III. *ITB Control*

III.1 Position control

It is often not easy to tell from the experimental profiles at exactly what point in time and space that an ITB has formed. The profiles of density and/or temperature typically show a break in the slope where it can be inferred that the transport is different on either side of this position or ITB "foot". In order to determine this location, Tresset[17] proposed using a dimensionless parameter ρ^*_T, defined to be the ratio of the Larmor radius at the ion sound speed (ρ_s) to the temperature gradient scale length L_T ($1/L_T=1/T\ dT/dr$) to locate the barrier. For the JET tokamak, a critical value of 0.014 is

exceeded when an ITB is present in the core plasma. Other experiments such as the FTU tokamak[18] have found that the ITBs are well characterized by this parameter using the same critical value of 0.014. This parameter is in effect a proxy for the ratio of the E x B shearing rate to the maximum linear growth rate of the pressure gradient driven modes.

On Alcator C-Mod, the break in slope indicating the presence of an ITB occurs in the density and pressure profiles, and is usually not observable in the electron temperature profile. (Ion temperature profile data are not available.) It has been demonstrated that using a dimensionless parameter similar to the one for the JET tokamak, ρ^*_P, which is defined as ρ_s/L_P where $1/L_p=1/P\ dP/dr$, can be used to locate the ITB position in Alcator C-Mod[5]. Here it is plotted as a function of radius in Fig.13a during the ITB phase of an Alcator C-Mod off-axis heated ITB plasma. It can be seen that although neither ρ^*_T nor $\rho^*_N = \rho_s/L_N$ exceeds the JET value of 0.014, ρ^*_P, which is the sum of the two, is higher than 0.014 in part of the core region of the plasma. Comparison of the location where ρ^*_P begins to exceed 0.014 to the position chosen for the ITB foot by an alternative method which calculates the derivatives of a functional fit to the data gives corresponding values for the location and onset time of the ITB. It should also be noted that at the point where $\rho^*_T = \rho^*_N$ the ratio of the density gradient scale length to the temperature gradient scale length (η_i) is equal to 1 and that this location also tends to be near the barrier location (in the example shown in Fig 13.a, $\eta_i = 1$ at the same location that $\rho^*_P = 0.014$). Contours of ρ^*_P as a function of major radius and time are shown in Fig. 13.b from the time of ITB onset. The position of the ITB foot determined from the density profile is shown in red. It lies very close to the $\rho^*_P = 0.014$ contour.

The location of the ITB foot in Alcator C-Mod has been shown to narrow with increasing toroidal magnetic field[6]. Results found by scanning the plasma current with a fixed magnetic field suggested that the foot position moved outward with increasing current [7]. The current dependence has now been tested at high magnetic field as well, and the result for two fields are shown in Fig 14a. A clear trend with both increasing plasma current and decreasing magnetic field is demonstrated. Fitting the data with a power law to these quantities results in r/a at the foot position ~ $I_p^{0.94}$ $B_t^{1.13}$. Since the q profile of the plasma depends upon the ratio of these quantities, the data is also plotted a function of q_{95} in Fig. 14b, showing a linear dependence of the ITB foot position with decreasing q_{95}. Comparison with the calculated q profile determined by EFIT shows that the typical ITB location lies between a q value of 1.1 and 1.34. (Note that these discharges are sawtoothing, and that the sawtooth inversion radius is well determined to be inside of the ITB foot location.)

III.2 Control of the Particle Accumulation

Typically, during the ITB phase of the Alcator C-Mod plasma, the particle and impurity influx is continuous until either the current is brought down to end the discharge or the radiation level increases to the point where the plasma undergoes a back transition to L-mode. It was demonstrated previously that this continued particle accumulation in the plasma core could be halted by the application of a small amount of central ICRF heating while preserving the ITB profile[3,4]. This has been demonstrated for ITBs

created with off-axis ICRF heating as well as for those arising spontaneously from Ohmic H-mode EDA conditions[6].

An example of this effect is shown in Fig 15. In this case similar Ohmic EDA H-mode ITB plasmas were developed, and then central ICRF heating was turned on late in the discharge. This demonstrated that increasing levels of ICRF could be used to control how high the central density was allowed to rise before it was clamped. In this experiment and similar ones with off-axis ICRF heating, it was also found that there was an apparent relatively low power limit (~0.8 MW) to how much additional ICRF power could be added without degrading or destroying the ITB profile. More recently ITB experiments which used a higher level of off-axis ICRF power have allowed a higher level of central ICRF power to be added while preserving the ITB. At this point, the central power which has been achieved appears to be limited only by the available source power, as long as the ratio of central to total power is maintained, as describe in section II.3.

Increasing the central power in this case resulted in strong central heating of the plasma, and record plasma pressure for Alcator C-Mod. Exemplary plasma performance parameters have been achieved in this manner[7]. An example is shown in Fig. 16 with the electron pressure profiles shown in Fig. 17. The ITB was established with off-axis ICRF power of 2.3 MW. Once established an additional 1.7 MW of central ICRF power was added. This caused a 5-fold increase in the fusion production of the plasma, along

with a doubling of the electron and ion temperatures as well as the plasma pressure. No degradation of the density peaking occurred.

IV. *Transport Analysis*

The particle and thermal transport characteristics of the ITB discharges have been determined through use of the TRANSP code[19] . These calculations use the electron density and temperature profiles from the experiment and use a variable multiplier on χ_i (Chang-Hinton[20]) to obtain the ion temperature profiles consistent with the measured neutron rate. The central ion temperature for these plasmas is very close to the electron temperature, which makes separation of the ion and electron thermal transport channels impossible due to the uncertainty in the exchange term. Thus, the behavior of an effective thermal transport coefficient, $\chi_{eff} \equiv \frac{n_e \chi_e \nabla T_e + n_i \chi_i \nabla T_i}{n_e \nabla T_e + n_i \nabla T_i}$, is reported here. As the ITB develops in these plasmas, the value of χ_{eff} in the core region decreases from the typical H-mode value of 1.1 - 1.4 m^2/s to 0.1 - 0.2 m^2/s, which is equivalent to the value of neoclassical ion thermal transport for these plasmas. This is shown in Fig. 18 for both a)off-axis ICRF heated and b) Ohmic H-mode ITB plasmas.

These plasmas often have sawtooth instability present throughout the development of the ITB. This allows use of the propagation rate of the heat pulse which occurs at the sawtooth crash to investigate further the thermal transport in these plasmas. A significant delay in the propagation of this heat pulse across the transport barrier regions has been reported [4] in the soft X-ray emission from what is observed during H-mode, as can be

seen in Fig. 19. This delay is best modeled by using a narrow region(<0.02 m) of reduced electron heat transport at or near the location of the ITB foot, determined from the electron density profile. This has been interpreted as a decrease in the incremental electron heat conductivity to a value of approximately 0.1 m^2/s at the barrier, consistent with the typical χ_{eff} determined by TRANSP calculation.

It is also noted that the particle diffusivity decreases as an ITB develops to a level similar to χ_{eff} in the core region[21]. This decrease in the outward particle diffusion allows the inward neoclassical pinch term to dominate the transport. The pinch term is sufficient to account for the experimentally observed central density increase[22,21]. The neoclassical pinch velocity is relatively large in Alcator C-Mod because the device is small compared to other tokamaks of this generation, resulting in a larger toroidal electric field. It also operates at somewhat lower electron temperature which further contributes to the pinch velocity. The impurity diffusion coefficient and velocity also tend towards neoclassical values during the ITB phase of the plasma.

The bootstrap current inside of the barrier region increases by as much as 10 times as the ITB develops and reaches a local value which is 10-12% of the Ohmically induced current. These values of ITB generated bootstrap current are obtained in both Ohmic EDA H-mode plasmas as well as for off-axis ICRF generated ITBs[3,6].

V. *Gyrokinetic Simulations and Analysis*

Ion thermal transport for typical Alcator C-Mod H-mode plasmas is thought to be dominated by turbulence resulting from ion temperature gradient driven modes[23]. The formation of a transport barrier in the plasma is believed to result from the reduction of this turbulent transport at the barrier and in the core. The reduced particle transport allows the neoclassical particle pinch to steadily peak the density profile for a duration lasting tens of energy confinement times.

Exploration of the drift wave stability in C-Mod ITB plasmas has been done using the GS2 code[24,25], which treats the gyrokinetic Vlasov-Maxwell equations as an initial value problem. Linear stability at the onset time of the ITB has been explored in depth[21,26,27], including mapping the evolution of the ITB trajectory through stability space [21]. Full non-linear modeling has been carried out for specific off-axis heated ITB cases which received supplemental central heating as a control mechanism[21,27].

At the onset time for the ITB, the barrier region is found to be marginally stable or stable to long wavelength toroidal ITG modes [21,26,27]. The addition of off-axis heating broadens the temperature profile, stabilizing ITG modes [27]. The evolution of the maximum linear growth rate at the position $\rho=0.4$, where ρ is the square root of the normalized toroidal flux ($\rho \sim r/a$), is shown in Fig. 20, along with the inverse density and temperature scale lengths and temperature[21,27]. It can be seen that at this position, which lies just to the inside of the ITB foot, the density gradient scale length is steadily decreasing after the onset of the EDA H-mode, which occurs just before t=0.8 s. The temperature gradient is just below marginal stability for toroidal ion temperature gradient

(ITG) modes this time of ITB onset. The ITG mode is strongly growing outside of the barrier, where the density gradient relatively flat, however. In this case, after t=1.0 s, when the ITB is fully established and the density scale length at ρ=0.4 is no longer rising, and the maximum linear growth rate becomes dominated by the trapped electron mode (TEM) which is driven by the steep density gradient. The change in the sign of the real frequency from the ion to the electron direction at this time, along with the disappearance of the mode when an adiabatic electron response is used, together with the insensitivity of the mode to the temperate gradient, confirm that the dominant instability has changed from ITG to TEM.

The peaking of the plasma density occurs when the core turbulent transport found in the non-linear simulation declines and the particle diffusivity decreases to a value near that of the effective heat diffusivity χ_{eff}[21]. The neoclassical (or Ware) pinch velocity is sufficiently strong in Alcator C-Mod to account for the central peaking of the density without requiring any anomalous pinch. This is evidenced by the observation that the particle diffusivity inferred from the continuity equation, using the calculated neoclassical pinch, remains positive for all time [21]. Accordingly, the nonlinear gyrokinetic simulations for the flat density gradient case, corresponding to early times, show an insignificant anomalous turbulent particle pinch, several orders of magnitude less than the Ware pinch[21]. As the density gradient increases, the turbulent particle flux changes from inward to outward.

The increasing density profile gradient is further stabilizing to toroidal ion temperature gradient driven modes, but at the same time is destabilizing to trapped electron modes (TEM) in the barrier region. The turbulent diffusivity from the TEM was found to increase with temperature in the gyro-Bohm manner, $D_e \propto T_e^{3/2}$ [21], with a weak departure due to collisionality effects. Thus even a small increase in the central power, as occurs with even a few hundred kW of on-axis ICRF, can contribute enough additional heating to cause the TEM driven turbulent transport inside of the barrier to balance the influx from the neoclassical pinch, which decreases with temperature. The balance between the collisional inflow and turbulent outflow results in a stable equilibrium [21]. The nonlinear gyrokinetic simulations of the TEM turbulence in this late quasi-steady phase reproduce the particle and energy fluxes inferred from transport analysis with measurement error, as shown in Fig. 21. This supports the picture that increased TEM turbulent outflow accompanies the addition of central ICRF power, which halts the density rise. The means of controlling the particle and impurity influx can be inferred from the temperature sensitivity of the equilibrium, revealed in the simulations [21].

Recently obtained results from phase-contrast imaging (PCI) measurements have shown the existence fluctuations in the density which appears to increase in intensity with the addition of central ICRF power into an ITB plasma[27]. The wave number and frequency are found to be consistent with the spectrum observed in the nonlinear turbulence simulations of one of these plasmas, although the PCI measurement cannot yet establish localization of this oscillation[28]. The relative increase in fluctuation intensity

during on-axis heating is in close agreeement with the simulations [27], however. Core fluctuations that appear to intensify with increasing density gradient during ITB plasmas have been reported from measurements using a heterodyne electron-cyclotron-emission diagnostic[29].

Several observations regarding the formation of the ITB are not yet understood. The slowing and sometime reversal of the central plasma rotation as the plasma becomes more peaked suggests that rotational shear may play a role. However, initially the ITB profile begins to build up when the plasma is in H-mode. The apparent velocity profiles at that time are typically flat (no velocity shear) from $0 < r/a < 0.6$[30,31], slightly outside of the ITB foot position $r/a \approx 0.45$ during the H-mode. The central velocity has been observed to decrease slightly earlier than that at larger radii during the ITB[30,31], an effect that needs to be studied in more detail when greater radial resolution in the measurement becomes available.

VI. *Discussion and Future Work*

The ITBs observed in Alcator C-Mod form spontaneously in the pressure profiles in EDA H-mode plasmas if the input power profile is broadly distributed across the plasma rather than centrally peaked. Short lived ITBs appear at the back-transition from H- to L-mode as well as following pellet injection in ICRF heated plasmas. Except in the case of pellet injection, these are formed in the absence additional particle or momentum sources

in the plasma. While the long-lived ITBs have only been seen in EDA H-modes, it is thought that the relevant parameter is the steadiness of the H-mode (ELM free H-modes tend to have frequent back-transitions in Alcator C-Mod) and that it has to last long enough for the neoclassical pinch velocity to peak the central density. Once the central density and impurities begin to peak, they will generally continue to rise until the H-mode collapses.

It has been demonstrated, however, that the addition of central ICRF power into an established ITB plasma will control the further rise of the central particle and impurity accumulation, likely through amplifying the trapped electron mode (TEM) driven turbulent transport. A bonus of this process is the increase in the central temperature, pressure and fusion rate in the core. Doubling of the central temperature and pressure (to 0.2 MP) and 10-fold increase in the fusion rate have been achieved.

The ITB foot location has been determined to depend on increasing plasma current and decreasing toroidal magnetic field, making it likely that the functional dependence is on the safety factor or magnetic shear.

The current program of research in C-Mod ITBs involves study of the role of critical temperature gradient, density profile, rotational shear and magnetic shear in the ITB onset. This program is being pursued both with the available experimental tools as well as in theory and modeling using the GS2 code. The role of density fluctuations will be explored with improved resolution of the PCI and reflectometry diagnostics in the short

term. The PCI diagnostic will be soon upgraded to allow the fluctuation measurement to be spatially located within the plasma.

The Alcator C-Mod program will soon begin operation of lower-hybrid wave current drive (LHCD) experiments. This will allow further exploration of the effects of tailoring of the q-profile on the ITB foot position. It will also provide information on the role of the neoclassical pinch in establishment of these ITBs, since this pinch is driven by the toroidal electric field which can be minimized or eliminated in LHCD experiments.

Acknowledgements

This work is support by D.o.E. Coop. Agreement DE-FC02-99ER54512. The authors would like to thank Amanda Hubbard (MIT), Alan Lynn (University of Nevada) and Perry Phillips (FRC, UT Austin) for high resolution electron temperature data, Dimitri Mossessian and Jerry Hughes for Thomson scattering density and pressure profiles. They would also like to thank Steve Wolfe, Joe Snipes, Bob Granetz, Ron Parker, Bill Rowan, and Jim Irby for their expert operation of the tokamak for many of the experiments presented here, Yijun Lin for operation of the ICRF system and also the Alcator C-Mod Operations Group for their support of this work.

References

[1]Rice J E *et al* 2001 *Nucl. Fusion* **41** 277

[2]Fiore C L *et al* 2001 *Phys Plasmas* **8** 2023

[3]Rice J E *et al* 2002 *Nucl. Fusion* **42** 510

[4]Wukitch S J *et al* 2002 *Phys. Plasmas* **9** 2149

[5]Rice J E *et al* 2003 *Nucl. Fusion* **43** 781

[6]Fiore C L *et al* 2004 *Phys. Plasmas* **10** 2480

[7]Fiore C L *et al* 2004 *Plasma Phys. Control. Fusion* **46** B281

[8]Greenwald M J *et al*. 1984 *Phys. Rev. Lett*. **53** 352

[9]Wolfe S M *et al.* 1986 *Nucl. Fus.* **26** 219

[10]Garnier D T *et al* 1996 *Proc. of the 16th International Conference on Fusion Energy* (Montreal,1996) (International Atomic Energy Agency, Vienna,1997), Vol. I,90.

[11]Takase Y *et al.* 1997 *Phys. Plasmas* **4** 1647

[12]Lao L *et al* 1985 *Nucl Fusion* **25** 1611

[13]Marmar E S *et al* 2001 Rev. Sci. Instrum.**72** 940

[14] Rice J E and Marmar E S 1995 *Rev. Sci. Instrum*. **66** 752

[15]Rice J E *et al* 1999 *Nucl. Fusion* **39** 1175

[16]Brambilla M 1999 *Plasma Phys. Controlled Fus.* **41** 1

[17] Tresset G *et al.* 2002 *Nucl. Fusion* **42**, 520

[18]Pericoli Ridolfini V *et al*. 2003 *Nucl. Fusion* **6** 469

[19]Hawryluk R 1979 in *Physics of Plasma Close to Thermonuclear Conditions* (Varennna,1979), Commission of the European Communities, Brussels, Vol. I p 61

[20]Chang C S and Hinton F L 1982 *Phys. Fluids* **25** 1493

[21]Ernst D R *et al* 2004 *Phys. Plasmas* **10** 2637

[22]Bonoli P T *et al* 2001 *Bull. Am. Phys. Soc.* **46** 54

[23]Greenwald M *et al* 1997 *Nucl. Fusion* **37** 793

[24]Kotschenreuther M *et al* 1995 *Comput. Phys. Commun.* **88** 129

[25]Dorland W *et al.* 2000 *Phys. Rev. Lett.* **85** 5579

[26]Redi M H *et al*., Proceedings EPS (2004) London, England Paper 2-163 and Redi M H *et al* "Microturbulent Drift Mode Stability before Internal Transport Barrier Formation in the Alcator C-Mod Radio Frequency Heated H-mode" accepted for publication in *Phys. Plasmas*

[27]Ernst D R *et al* 2004 *Proc. of the 20th IAEA Fusion Energy Conference* (IAEA, Vilamoura, Portugal,2004) TH/4-1 http://www-naweb.iaea.org.napc/physics/fec/fec2004/datasets/th4-1.html

[28]Basse N P *et al* 2005 *Phys. Plasmas* **12** 052512

[29]Lynn AG *et al* "Density and Temperature Fluctuations in Alcator C-Mod Plasmas with Peaked Density Profiles" submitted to *Phys. Plasmas*

[30]Lee W D *et al* 2003 *Phys Rev. Lett*. **91** 205003

[31]Rice J E *et al* 2004 *Nucl. Fusion* **44** 379

Figure captions

Fig. 1. The plasma parameters are shown for a typical PEP mode shot.

Fig. 2. The density profiles (a) and the global neutron rate (b) are shown for a PEP mode plasma. The peak in the neutron rate comes during the reheating of the plasma as the density is relaxing towards the pre-pellet value.

Fig. 3. The density profile collapses at the H to L-mode transition (a) in enhanced neutron (EN) mode; An ITB profile forms (b) and then returns to a flat profile (c). The neutron rate rises sharply during the ITB, then relaxes after the density profile once again becomes flat. Note that the neutron rate (i.e. ion temperature) relaxes more slowly than the density profile.

Fig. 4. Typical plasma parameters are shown for an EN mode. Along with the neutron rate increase, the central ion and electron temperatures increase while the line average density drops. Central plasma pressure increases while there is a short lived decrease in the plasma stored energy which then recovers well before the plasma returns to H-mode.

Fig. 5. Ion and electron temperature profiles are shown before and during the ITB phase of the EN mode discharge. The temperatures increase, but the profile shape is maintained.

Fig. 6. The ratio of electron temperature scale length to electron density scale length decreases to a value near 1 at the plasma half radius as the fusion neutron rate peaks in EN mode plasmas.

Fig 7. Profiles of the square root of the visible bremsstrahlung emission are shown during an ITB formed with off-axis ICRF heating. A calculation of the RF deposition profile is included for comparison.

Fig. 8. Zeff derived from obtaining the ratio of the square root of the visible bremsstrahlung emission to the density from Thomson scattering is shown as a function of a) position and b) time.

Fig. 9. The rotation velocity is compared for a standard H-mode with a plasma which develops an ITB, as is seen from the peaking of the density profile.

Fig. 10. Central plasma rotation and density peaking factor for a toroidal field scan with 70 Mhz ICRF power.

Fig. 11. The toroidal magnetic field is ramped either up or down (a) moving the ICRF resonance towards or away from the center of the plasma. The percentage of power inside the ITB radius (b) changes with the resonance position and the point where an ITB is either formed or lost is indicated.

Fig. 12. Density profiles are shown as an ITB develops in a purely Ohmic EDA H-mode.

Fig. 13. The dimensionless parameters ρ^*_T, ρ^*_n, and ρ^*_p are shown as a function of radius (a) when a typical ITB profile is present in the plasma; (b)contours of ρ^*_p are plotted as a function of major radius and time.

Fig. 14. The ITB foot position decreases with increasing toroidal magnetic field and decreasing plasma current.

Fig. 15. Incremental central ICRF power is added to established ohmic H-mode ITBs over several shots: a.) density profiles; b.) final density decrease with increasing input power.

Fig. 16. Plasma parameters for a high performance ITB discharge with added central ICRF power.

Fig. 17. Electron pressure profiles during the shot shown in Fig 15. Strong pressure peaking is achieved with the addition of central ICRF.

Fig. 18 χ_{eff} in the core region decreases to the neoclassical ion thermal transport during an ITB for both a)off-axis ICRF heated and b) Ohmic H-mode ITB plasmas

Fig. 19 During an ITB the heat pulse resulting from a sawtooth crash is delayed in its propagation from what is seen during H-mode.

Fig. 20. Temporal evolution of a) maximum linear growth rate, radial electric field shearing rate, and real frequency at the ITB radius (ρ=0.4); b) temperature at the ITB radius; c) inverse density gradient scale length from visible bremsstrahlung data; d) effective particle diffusivity inside the ITB foot, from density profile measurements and calculated Ware pinch.

Fig. 21. Comparison of simulated and measured transport, at ρ=0.4, t=1.2 s accounting for Z_{eff} gradients as functions of a/L_{ne} from linear GS2 simulations: a) maximum growth rate and real frequency; b)poloidal wave number $k_\theta\rho_i$ yielding the maximum linear growth rate; c)particle flux and d) particle diffusivity from TEM turbulence equals that from the Ware pinch for a/L_{ne}=1.47; e)effective thermal diffusivity matches the TRANSP value at $1/L_{ne}$=1.72, all within experimental error.

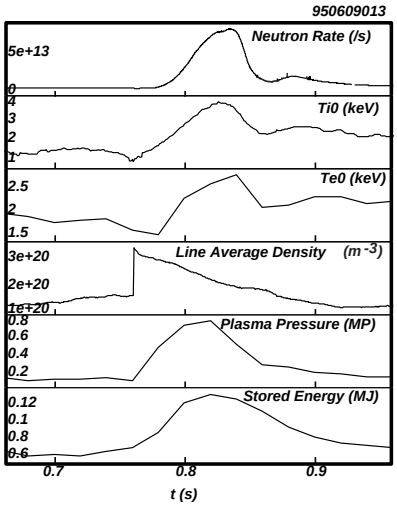
950609013
Neutron Rate (/s)
5e+13
0
Ti0 (keV)
4
3
2
1
Te0 (keV)
2.5
2
1.5
Line Average Density (m -3)
3e+20
2e+20
1e+20
Plasma Pressure (MP)
0.8
0.6
0.4
0.2
Stored Energy (MJ)
0.12
0.1
0.8
0.6
0.7
0.8
0.9
t (s)

Figure 1.

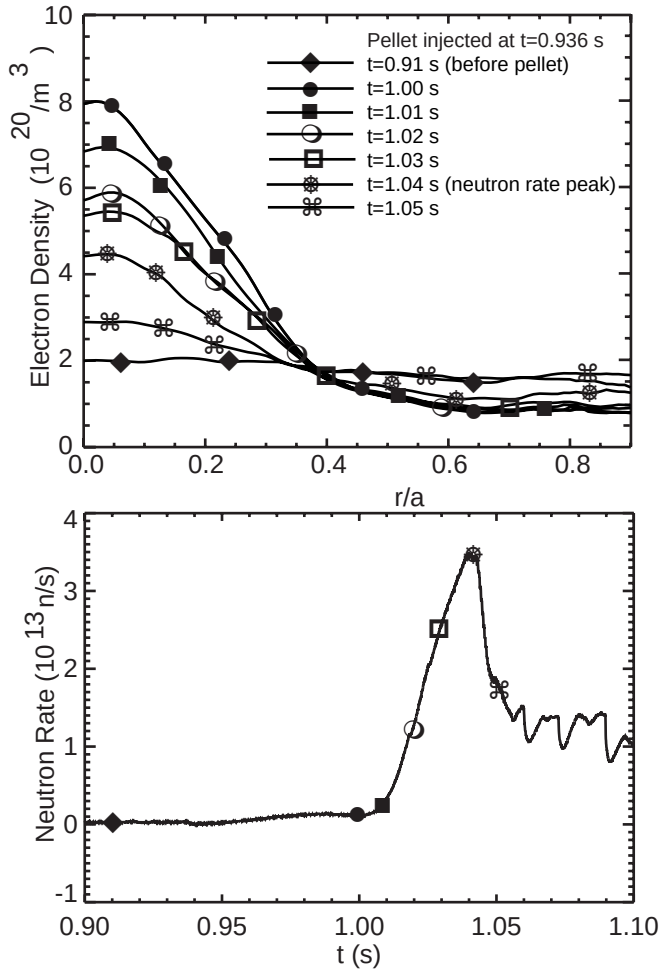
Pellet injected at t=0.936 s
t=0.91 s (before pellet)
t=1.00 s
t=1.01 s
t=1.02 s
t=1.03 s
t=1.04 s (neutron rate peak)
t=1.05 s
Electron Density (10^20/m^3)
r/a
Neutron Rate (10^13 n/s)
t (s)

Figure 2.

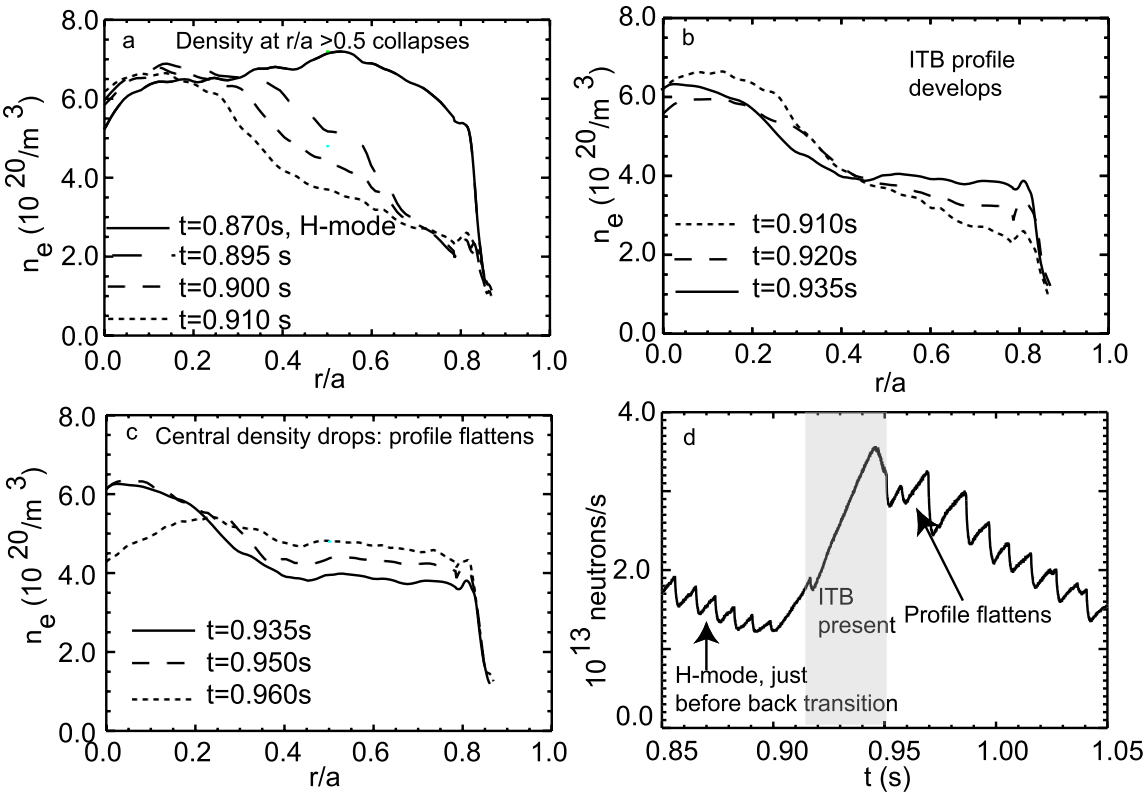
a
Density at r/a >0.5 collapses
t=0.870s, H-mode
t=0.895 s
t=0.900 s
t=0.910 s
b
ITB profile develops
t=0.910s
t=0.920s
t=0.935s
c
Central density drops: profile flattens
t=0.935s
t=0.950s
t=0.960s
d
ITB present
Profile flattens
H-mode, just before back transition
r/a
t (s)

Fig. 3.

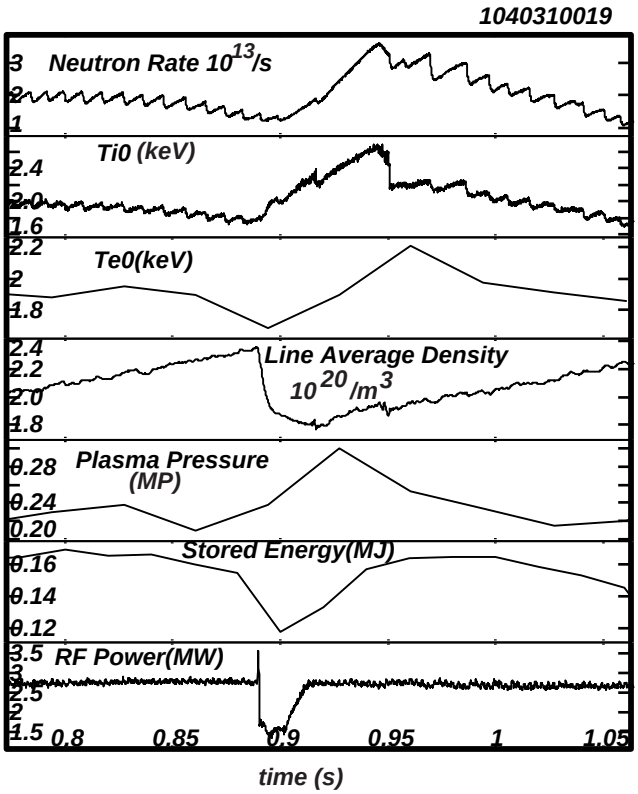
1040310019
Neutron Rate 10^13/s
3
2
1
Ti0 (keV)
2.4
2.0
1.6
Te0(keV)
2.2
2
1.8
Line Average Density
10^20/m^3
2.4
2.2
2.0
1.8
Plasma Pressure
(MP)
0.28
0.24
0.20
Stored Energy(MJ)
0.16
0.14
0.12
RF Power(MW)
3.5
3
2.5
2
1.5
0.8
0.85
0.9
0.95
1
1.05
time (s)

Fig. 4.

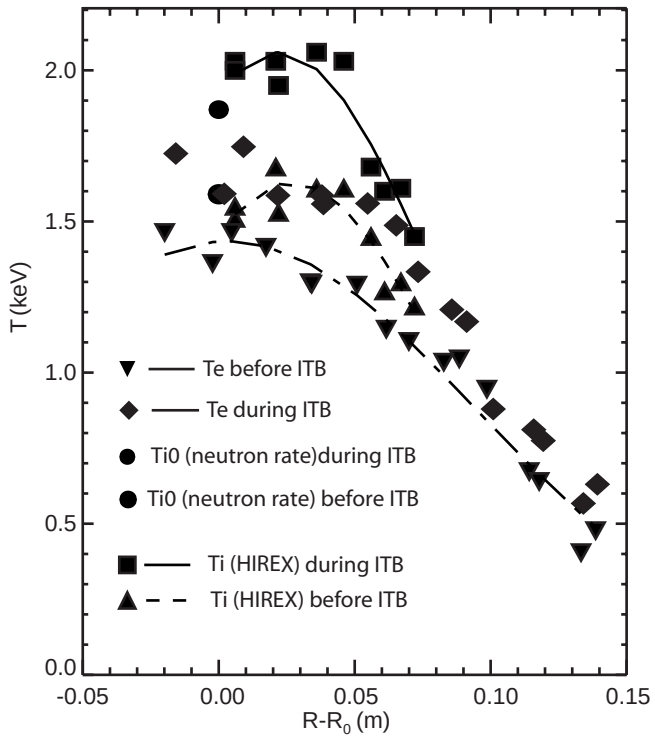
T (keV)
2.0
1.5
1.0
0.5
0.0
-0.05
0.00
0.05
0.10
0.15
R-R0 (m)
Te before ITB
Te during ITB
Ti0 (neutron rate)during ITB
Ti0 (neutron rate) before ITB
Ti (HIREX) during ITB
Ti (HIREX) before ITB

Fig. 5

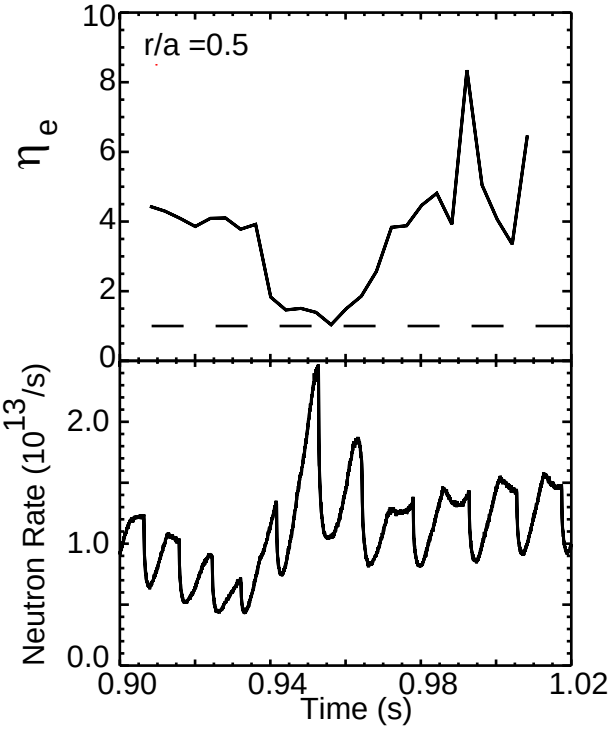
r/a =0.5
η_e
Neutron Rate (10^{13}/s)
Time (s)
0
2
4
6
8
10
0.0
1.0
2.0
0.90
0.94
0.98
1.02

Fig. 6

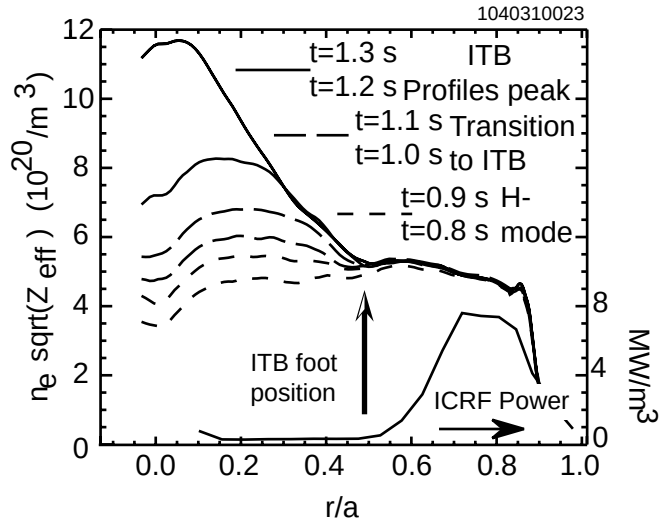
1040310023
t=1.3 s
t=1.2 s
t=1.1 s
t=1.0 s
t=0.9 s
t=0.8 s
ITB
Profiles peak
Transition
to ITB
H-
mode
ITB foot
position
ICRF Power
n_e sqrt(Z_{eff}) (10^{20}/m^3)
MW/m3
r/a
0
2
4
6
8
10
12
0.0
0.2
0.4
0.6
0.8
1.0

Fig. 7.

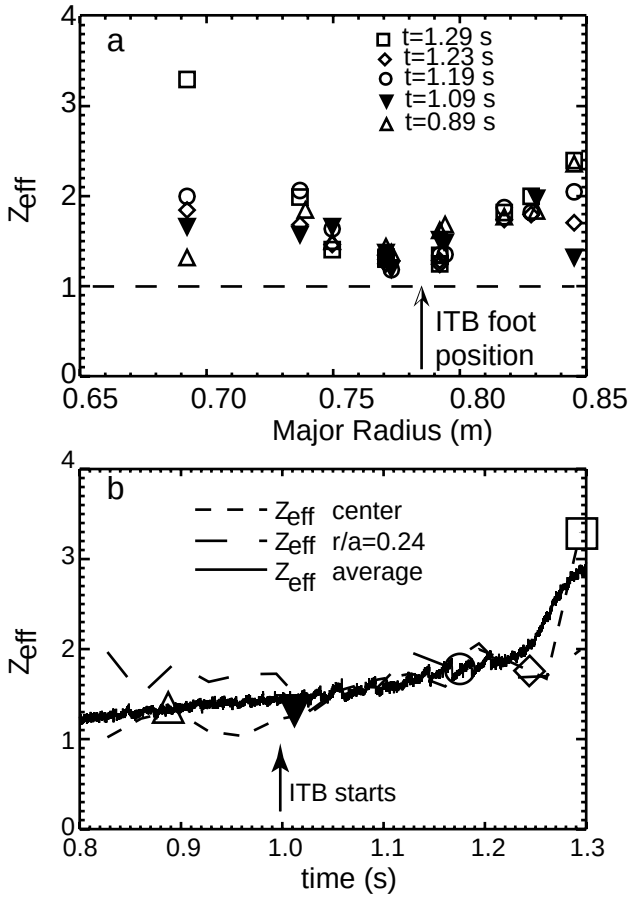
a
t=1.29 s
t=1.23 s
t=1.19 s
t=1.09 s
t=0.89 s
ITB foot
position
Z_eff
Major Radius (m)
b
Z_eff center
Z_eff r/a=0.24
Z_eff average
ITB starts
Z_eff
time (s)

Fig. 8

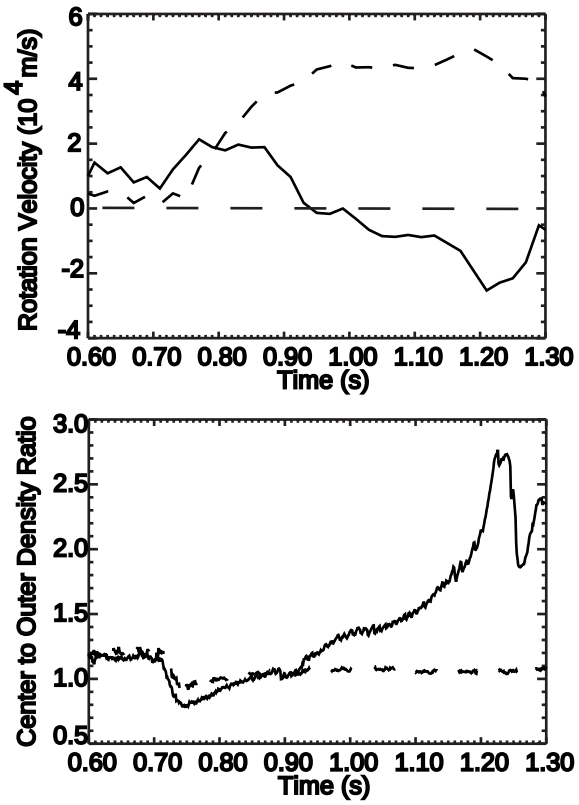
Rotation Velocity (10^4 m/s)
6
4
2
0
-2
-4
0.60 0.70 0.80 0.90 1.00 1.10 1.20 1.30
Time (s)
Center to Outer Density Ratio
3.0
2.5
2.0
1.5
1.0
0.5
0.60 0.70 0.80 0.90 1.00 1.10 1.20 1.30
Time (s)

Fig. 9

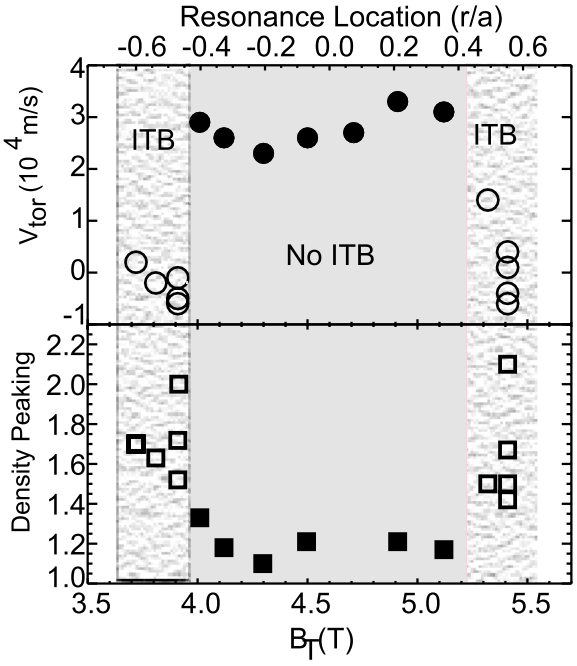
Resonance Location (r/a)
-0.6 -0.4 -0.2 0.0 0.2 0.4 0.6
V_{tor} (10^4 m/s)
ITB
No ITB
ITB
Density Peaking
3.5 4.0 4.5 5.0 5.5
B_T(T)

Fig. 10

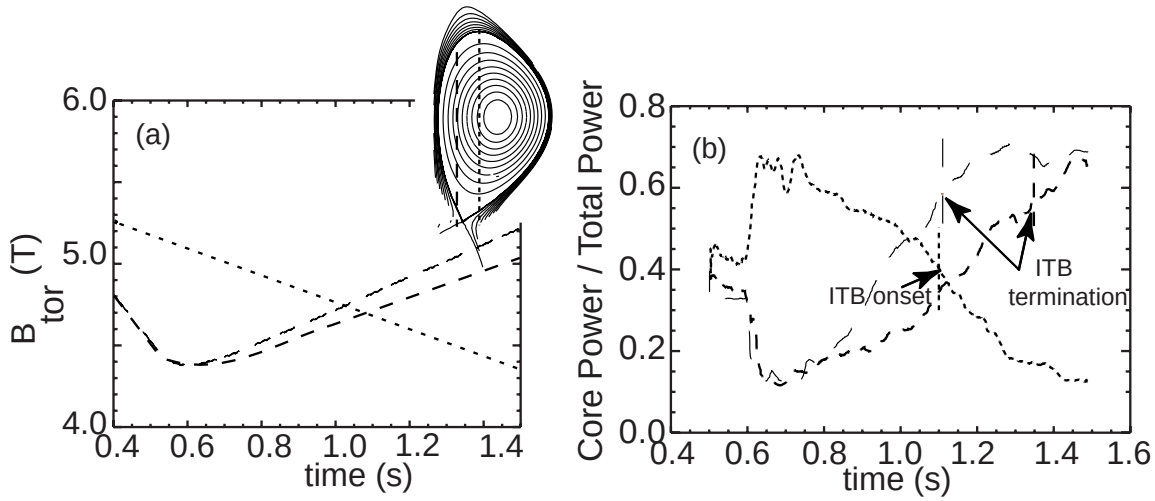
(a)
6.0
5.0
4.0
B tor (T)
0.4
0.6
0.8
1.0
1.2
1.4
time (s)
(b)
0.8
0.6
0.4
0.2
0.0
Core Power / Total Power
ITB onset
ITB
termination
0.4
0.6
0.8
1.0
1.2
1.4
1.6
time (s)

Fig. 11

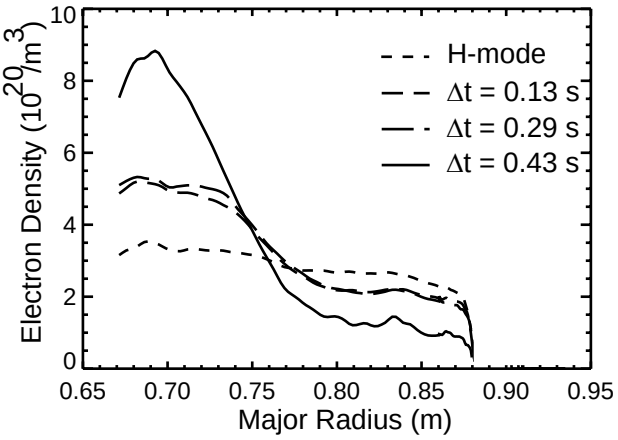
Electron Density (10^{20}/m^3)
Major Radius (m)
H-mode
Δt = 0.13 s
Δt = 0.29 s
Δt = 0.43 s
0
2
4
6
8
10
0.65
0.70
0.75
0.80
0.85
0.90
0.95

Fig 12

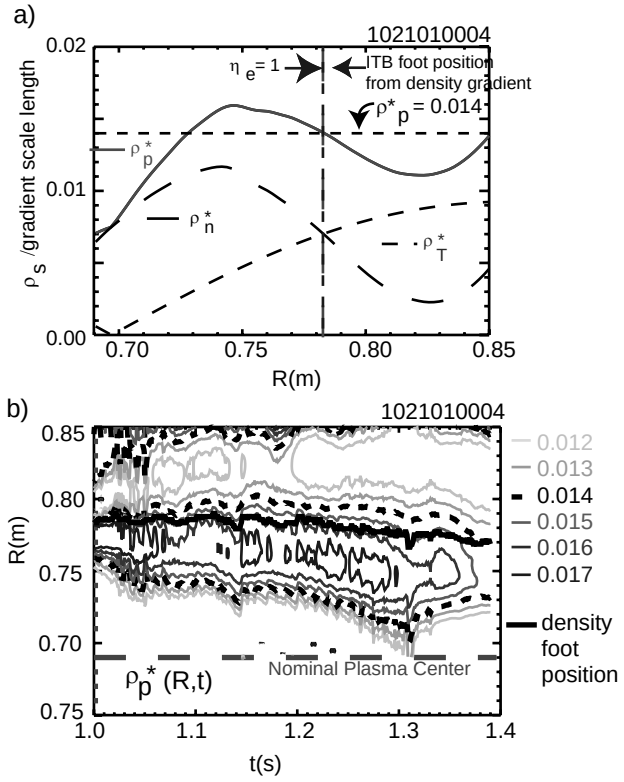
a)
1021010004
0.02
0.01
0.00
$\eta_e = 1$
ITB foot position
from density gradient
$\rho^*_p = 0.014$
ρ^*_p
ρ^*_n
ρ^*_T
ρ_s /gradient scale length
0.70
0.75
0.80
0.85
R(m)
b)
1021010004
0.85
0.80
0.75
0.70
0.75
R(m)
0.012
0.013
0.014
0.015
0.016
0.017
density
foot
position
ρ_p^* (R,t)
Nominal Plasma Center
1.0
1.1
1.2
1.3
1.4
t(s)

Fig 13

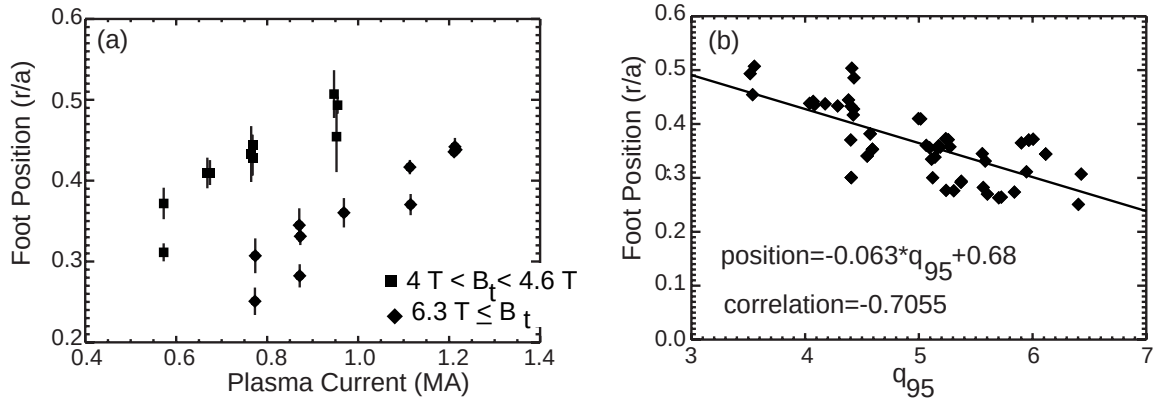
(a)
Foot Position (r/a)
Plasma Current (MA)
4 T < B_t < 4.6 T
6.3 T ≤ B_t
(b)
Foot Position (r/a)
position=-0.063*q95+0.68
correlation=-0.7055
q95

Fig 14

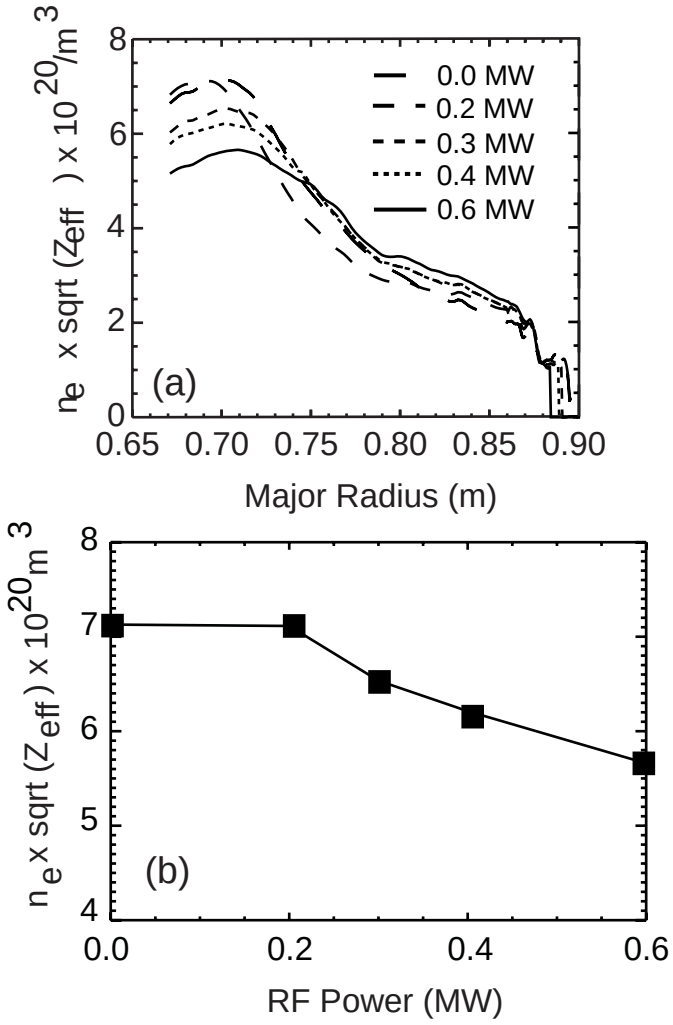

Fig 15

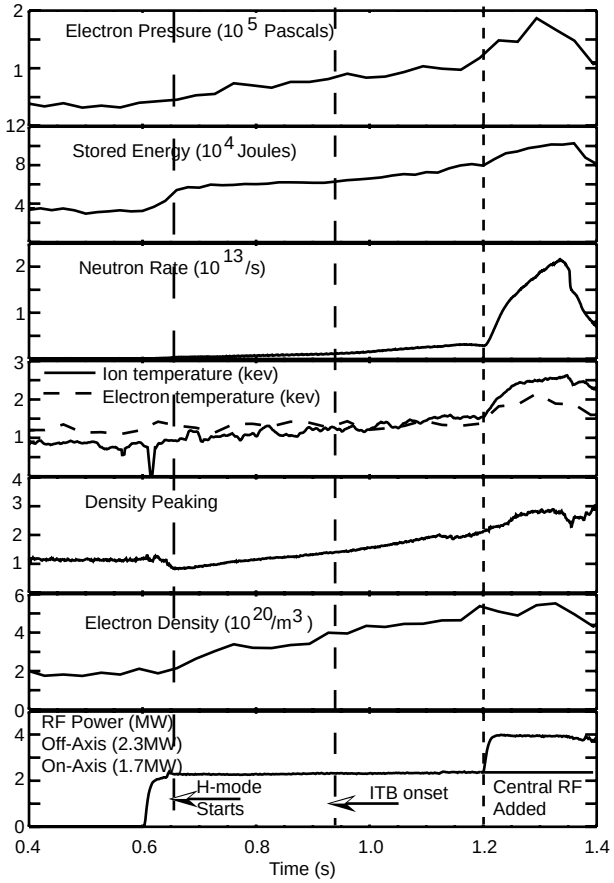
Electron Pressure (10^5 Pascals)
Stored Energy (10^4 Joules)
Neutron Rate (10^13/s)
Ion temperature (kev)
Electron temperature (kev)
Density Peaking
Electron Density (10^20/m^3)
RF Power (MW)
Off-Axis (2.3MW)
On-Axis (1.7MW)
H-mode Starts
ITB onset
Central RF Added
Time (s)

Fig 16

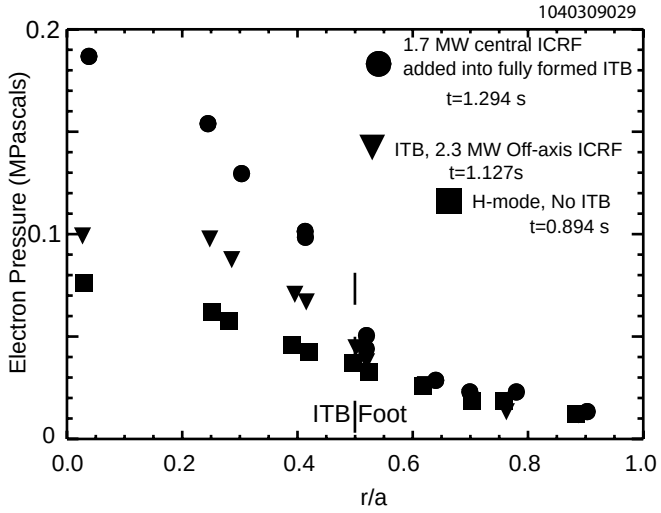
1040309029
1.7 MW central ICRF
added into fully formed ITB
t=1.294 s
ITB, 2.3 MW Off-axis ICRF
t=1.127s
H-mode, No ITB
t=0.894 s
ITB
Foot
Electron Pressure (MPascals)
r/a
0
0.1
0.2
0.0
0.2
0.4
0.6
0.8
1.0

Fig 17

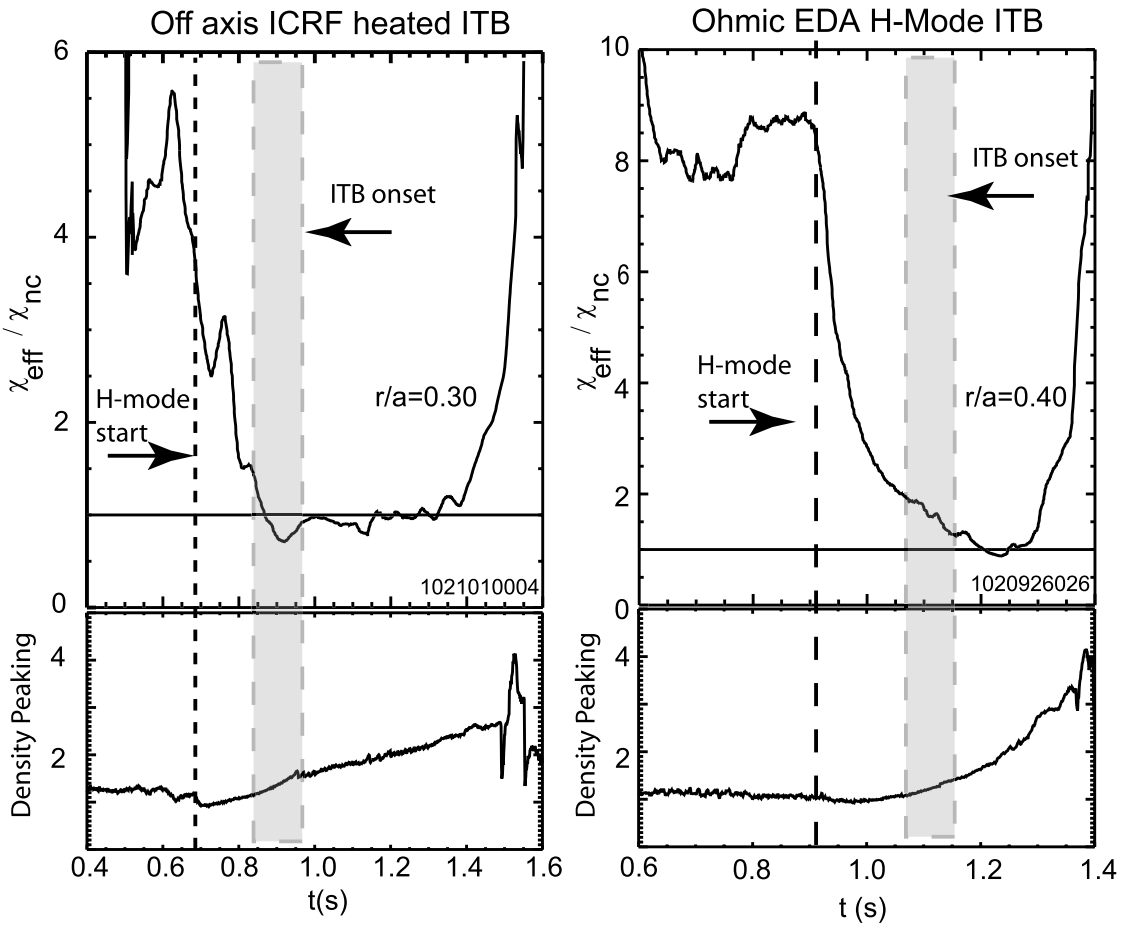
Off axis ICRF heated ITB
Ohmic EDA H-Mode ITB
ITB onset
H-mode start
r/a=0.30
r/a=0.40
1021010004
Density Peaking
t(s)
t (s)

Fig 18

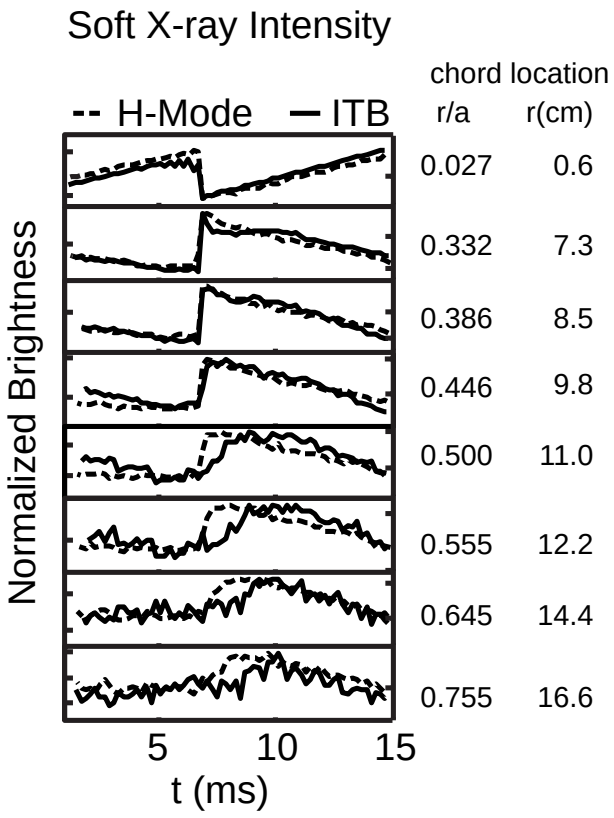
Soft X-ray Intensity
chord location
-- H-Mode — ITB
r/a
r(cm)
0.027
0.6
0.332
7.3
0.386
8.5
0.446
9.8
0.500
11.0
0.555
12.2
0.645
14.4
0.755
16.6
Normalized Brightness
5
10
15
t (ms)

Fig. 19

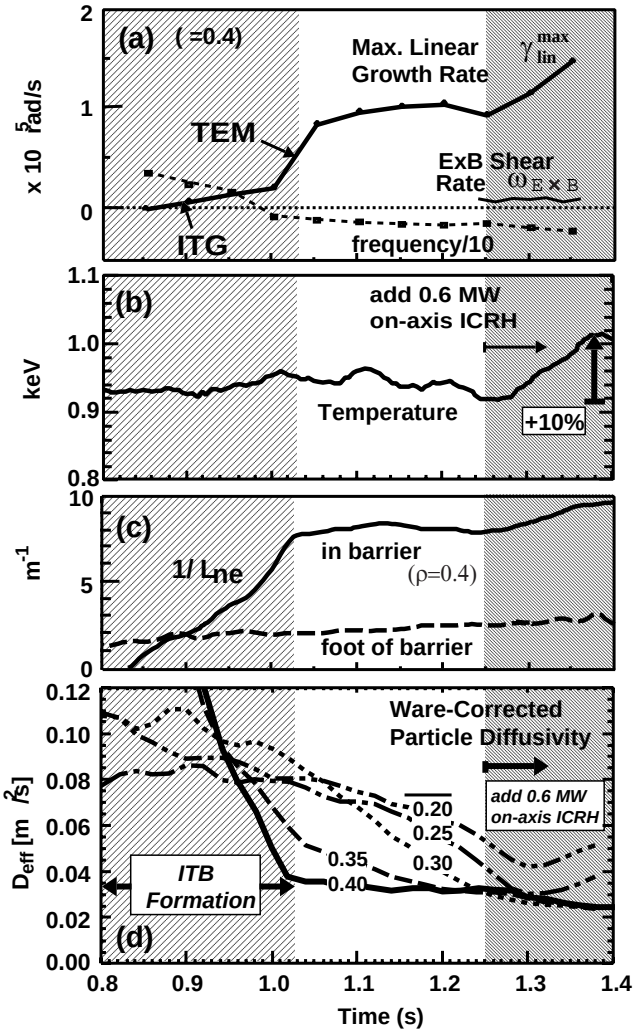
(a) (=0.4)
Max. Linear Growth Rate
γ_{lin}^{max}
TEM
ExB Shear Rate $\omega_{E\times B}$
ITG
frequency/10
x 10^5 rad/s
(b)
add 0.6 MW on-axis ICRH
Temperature
+10%
keV
(c)
1/ L_ne
in barrier
(ρ=0.4)
foot of barrier
m^-1
Ware-Corrected Particle Diffusivity
0.20
0.25
0.30
0.35
0.40
add 0.6 MW on-axis ICRH
ITB Formation
(d)
D_eff [m^2/s]
Time (s)

Fig. 20

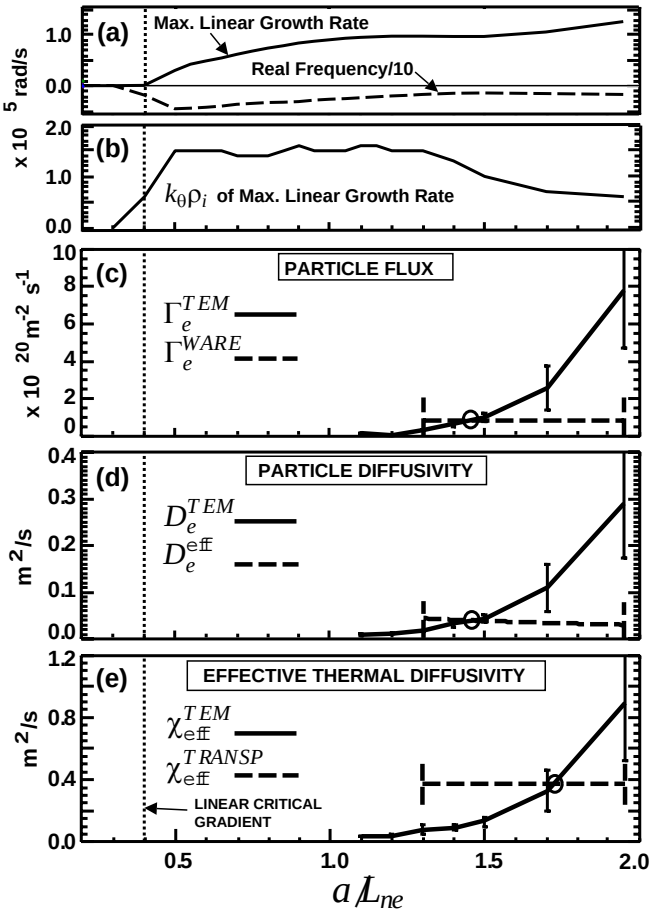
(a)
Max. Linear Growth Rate
Real Frequency/10
x 10^5 rad/s
1.0
0.0
(b)
$k_\theta \rho_i$ of Max. Linear Growth Rate
x 10^2
2.0
1.0
0.0
(c)
PARTICLE FLUX
Γ_e^{TEM}
Γ_e^{WARE}
x 10^20 m^-2 s^-1
10
8
6
4
2
0
(d)
PARTICLE DIFFUSIVITY
D_e^{TEM}
D_e^{eff}
m^2/s
0.4
0.3
0.2
0.1
0.0
(e)
EFFECTIVE THERMAL DIFFUSIVITY
χ_{eff}^{TEM}
χ_{eff}^{TRANSP}
LINEAR CRITICAL GRADIENT
m^2/s
1.2
0.8
0.4
0.0
0.5
1.0
1.5
2.0
a/L_{ne}

Fig. 21